Utility of ^{222}Rn as a passive tracer of subglacial distributed system drainage

Linhoff, Benjamin S.[1]; Charette, Matthew A.[1]; Nienow, Peter W.[2]; Wadham, Jemma L.[3]; Tedstone, Andrew J.[3]; Cowton, Thomas[2]

1: Department of Marine Chemistry and Geochemistry, Woods Hole Oceanographic Institution, Woods Hole, Massachusetts, USA
2: School of Geosciences, University of Edinburgh, Edinburgh, United Kingdom
3: School of Geographical Sciences, University of Bristol, Bristol, United Kingdom

Corresponding author: Benjamin Linhoff (blinhoff@usgs.gov)

Keywords: radon, Greenland, glacier, proglacial river, meltwater.

Abstract

Water flow beneath the Greenland Ice Sheet (GrIS) has been shown to include slow-inefficient (distributed) and fast-efficient (channelized) drainage systems, in response to meltwater delivery to the bed via both moulins and surface lake drainage. This partitioning between channelized and distributed drainage systems is difficult to quantify yet it plays an important role in bulk meltwater chemistry and glacial velocity, and thus subglacial erosion. Radon-222, which is continuously produced via the decay of ^{226}Ra, accumulates in meltwater that has interacted with rock and sediment. Hence, elevated concentrations of ^{222}Rn should be indicative of meltwater that has flowed through a distributed drainage system network. In the spring and summer of 2011

and 2012, we made hourly ^{222}Rn measurements in the proglacial river of a large outlet glacier of the GrIS (Leverett Glacier, SW Greenland). Radon-222 activities were highest in the early melt season (10-15 dpm L^{-1}), decreasing by a factor of 2-5 (3-5 dpm L^{-1}) following the onset of widespread surface melt. Using a ^{222}Rn mass balance model, we estimate that, on average, greater than 90% of the river ^{222}Rn was sourced from distributed system meltwater. The distributed system ^{222}Rn flux varied on diurnal, weekly, and seasonal time scales with highest fluxes generally occurring on the falling limb of the hydrograph and during expansion of the channelized drainage system. Using laboratory based estimates of distributed system ^{222}Rn, the distributed system water flux generally ranged between 1-5% of the total proglacial river discharge for both seasons. This study provides a promising new method for hydrograph separation in glacial watersheds and for estimating the timing and magnitude of distributed system fluxes expelled at ice sheet margins.

1 Introduction

Beneath the ablation zone of the Greenland Ice Sheet (GrIS), meltwater flow paths influence glacier velocities and bulk meltwater chemistry (Bartholomew et al., 2011a; Bartholomew et al., 2012; Tedstone et al., 2013; Hawkings et al., 2014). After the onset of spring melt, the majority of surface derived meltwater travels to the glacier or ice sheet bed through fractures, crevasses and moulins (Sharp et al., 1993; Das et al., 2008). During the summer, bulk meltwater is largely composed of two components, channelized drainage and distributed drainage, which are both derived from snow and ice melt (Tranter et al., 1993; Collins 1979; Chandler et al., 2013; Cowton et al., 2013). On the time scale of an entire melt season, the major component is channelized flow, which pertains to meltwater moving efficiently through large

47 basal channels (Röthlisberger, 1972; Nye, 1973). In contrast, distributed drainage refers to
48 meltwater in slow transit through either cavities that open behind bedrock bumps due to ice
49 sliding (linked-cavity system; Walder, 1986), a water sheet of near uniform thickness at the ice
50 bed (Creyts and Schoof, 2009), or water flow through permeable subglacial till (Boulton et al.,
51 2009). Meltwater traveling through distributed systems influences subglacial hydraulic pressure
52 distribution, channel spacing, basal sliding and bed deformation (Boulton et al., 2009; Rempel,
53 2009). In general, meltwater in the distributed system tends to have elevated dissolved solid
54 concentrations, a feature exploited by early attempts at hydrograph separation in glacial
55 watersheds (Collins, 1979). However, rapid mineral weathering reactions may occur when
56 sediments traveling through closed, CO_2 limited, distributed systems mix with open-system, low
57 ionic strength channelized meltwater (Raiswell, 1984; Tranter et al., 1993; Sharp et al., 1993).
58 Consequently, solute concentrations, often inferred through electrical conductivity (EC)
59 measurements, cannot unequivocally be used as conservative tracers of distributed system
60 meltwaters.

61 Radon-222 has been used extensively to examine groundwater-surface water exchange
62 processes in a wide range of freshwater and marine systems; this is because groundwater ^{222}Rn
63 activities are typically highly enriched relative to surface waters due to radioactive decay of
64 ^{226}Ra, naturally present in aquifer mineral surfaces (Burnett and Dulaiova, 2003; Cook
65 et al., 2003; Dulaiova et al., 2008; McCallum et al., 2012). As a relatively soluble, inert noble
66 gas that does not participate in biogeochemical or weathering reactions once in solution, ^{222}Rn
67 ($t_{1/2}$ = 3.82 days) can only be added to glacial meltwater in measurable quantities from extensive
68 water-rock interactions. Hence, by its nature, distributed system meltwater should acquire
69 significantly higher ^{222}Rn activities than meltwater that flows through open channels.

Discrete ^{222}Rn measurements in small glacial watersheds have been used to infer the transition from distributed to channelized drainage (Kies et al., 2010; Bhatia et al., 2011; Kies et al., 2015). This paper expands upon these earlier studies by examining the utility of long term continuous ^{222}Rn measurements in the proglacial river of a large GrIS outlet glacier during the spring and summer of 2011 and 2012. Using a detailed mass balance modeling approach, we provide evidence that ^{222}Rn is a passive tracer of subglacial hydrological routing that can be used to infer the timing and magnitude of distributed system fluxes. To our knowledge this is the first time that continuous, high-resolution ^{222}Rn measurements have been reported from a proglacial river over the course of a melt season.

2 Methods

2.1 Study Area

Fieldwork was conducted during the 2011 and 2012 melt seasons at Leverett Glacier, a large land-terminating glacier on the western margin of the GrIS (67º03'57.81"N, 50º10'01.83"; Figure 1). Its hydrological catchment covers >600 km^2, reaches an elevation of 1500 m, and ranges in width from 10-40 km (Bartholomew et al., 2011). Meltwater from the catchment is channeled through a single large proglacial river (Leverett River); at peak discharge, typical flows from the river are in the range of 300-400 $m^3\ s^{-1}$ (Bartholomew et al., 2010; Cowton et al., 2012). During an exceptional melting period in 2012, the river reached ~800 $m^3\ s^{-1}$ (Tedstone et al., 2013). On the south side of Leverett Glacier's snout, the bedrock is a late Achaean (2.5 Ga) granite (Escher, 1971; Nutman et al., 2010) while the Ikertoq complex (1.85 Ga), composed of basement gneisses and granites, borders the north side (Henriksen et al., 2000). The proglacial valley is filled with quaternary sediments composed of weathered materials from afore

93 mentioned rock units (Hindshaw et al., 2014). This suggests that the subglacial lithology is
94 similar to the bedrock adjacent to the glacier's snout.
95
96 *2.2 Discharge, conductivity, suspended sediment, and ^{226}Ra measurements*
97 Proglacial river discharge was measured using continuous water stage monitoring
98 through a stable bedrock section of the river (Sole et al., 2013; Tedstone et al., 2013). Stage was
99 converted to discharge using a continuous stage-discharge curve created from repeat Rhodamine
100 WT and Rhodamine B dye injections throughout both melt seasons; the normalized root mean
101 squared deviation of the discharge record has been estimated to be ±10% (Tedstone et al. 2013).
102 Concurrent measurements of EC and the suspended sediment concentration (SSC) are also
103 presented here and, for 2011 and 2012 data, in Butler (2014) and Hawkings et al. (2014)
104 respectively. EC was recorded every five minutes using a Campbell Scientific 247 combined
105 temperature-EC sensor, and logged using Campbell Scientific CR1000 and CR800 loggers. EC
106 was calibrated using a KCl solution of known concentration; errors on EC measurements were
107 ±10% (1-sigma). SSC was estimated from turbidity measurements made with a Partech IR 15C
108 turbidity probe. Calibration curves were created from discrete suspended sediment samples
109 collected from the river. Errors on SSC were ±6% (1-sigma). Dissolved ^{226}Ra was measured
110 throughout the 2011 and 2012 field seasons using methods described by Charette et al. (2001).
111 Briefly, ~200 L river samples were filtered through a column packed with MnO_2 impregnated
112 fiber. The fiber was ashed, packed in a sealed plastic vial, and counted for 2-3 days on a well-
113 type germanium gamma detector (Canberra) calibrated using a NIST ^{226}Ra standard prepared in
114 the same manner as the samples.
115

116 *2.3 Measuring radon in the proglacial river*

117 Radon-222 was measured in the Leverett Glacier proglacial river during 2011 (May 8-
118 August 5) and 2012 (May 12-July 28). Continuous (hourly) measurements were made using a
119 RAD7 (Durridge Inc.) radon-in-air monitor in series with a desiccant chamber and a RAD7
120 water probe, a submersible air-filled gas-permeable membrane coil made from Accruel® tubing
121 (henceforth the term "water probe" will refer to the ^{222}Rn extraction unit). River water ^{222}Rn
122 equilibrates with air in the membrane coil through passive diffusion; the air is continuously
123 circulated in a closed loop through the RAD7 radon-in-air monitor system (Hofmann et al., 2011;
124 Schubert et al., 2012). Radon-in-air activities were then converted to radon-in-water activity via
125 the temperature dependent air–water partition coefficient as described by Schubert et al. (2012).
126 The water probe was deployed on the northern bank of the river as close to the glacier's terminus
127 as possible (0-1 km) to minimize potential evasion of ^{222}Rn from the river to the atmosphere
128 (Supplementary Material). Rising river stage required that we periodically moved the water
129 probe downstream to a more stable riverbank. There was no observed decrease in effectiveness
130 of the water probe during long term deployment (Supplementary Material). Typical 1-sigma
131 counting errors for the water probe ^{222}Rn activities were ±5-20%. Discrete ^{222}Rn samples were
132 collected upstream of the water probe at the ice sheet terminus in 250 mL bottles and analyzed
133 using a RAD7 plus Rad-H_2O attachment on a regular basis (Figure S1; Supplementary Material).
134 These discrete ^{222}Rn samples agree within the counting errors of the corresponding continuous
135 ^{222}Rn measurements (Figure S1; Supplementary Material).

136 Measurements of ^{222}Rn via the water probe system may lag actual aqueous ^{222}Rn due to
137 the time required to equilibrate ^{222}Rn across the gas-permeable membrane (Schubert et al., 2012).
138 To assess the magnitude of this offset, we analyzed field equilibration times during instrument

startup and performed laboratory experiments to estimate the water probe's response time to changes in ^{222}Rn activity. Key factors that control the equilibration time include the air volume in the system (RAD7 unit, tubing, desiccant and membrane coil), the membrane coil surface area, and the ^{222}Rn activity gradient across the membrane water/air interface (Schubert et al., 2012). The equilibration time can be minimized when the air volume of the system is low (i.e. using less tubing between RAD7 and membrane), the membrane interface area is maximized (i.e. lengthening the membrane tubing), and the water/air ^{222}Rn activity gradient across the membrane coil is large. The ^{222}Rn activity gradient at the membrane water/air interface has by far the largest effect on the equilibration and response time of the water probe; in stagnant water the response time is on the order of several hours (Hofmann et al., 2011; Schubert et al., 2012). In a flowing river, the activity gradient at the water/air interface is close to 100% such that the response time can be reduced to <1 hour, similar to results obtained using a spray chamber equilibrator such as the RAD-Aqua (Durridge Inc.; Schubert et al., 2012). In our case, the equilibration time of the water probe in the proglacial river was determined to be no greater than 2 hours based on laboratory experiments and less than 1 hour in field observations. A detailed description of these tests and associated results is presented in the Supplementary Material.

2.4 ^{222}Rn in subglacial distributed systems and sediment properties

Because we were unable to obtain *in-situ* distributed system samples from beneath the ice sheet, we estimated ^{222}Rn in this environment via laboratory-based equilibration experiments (Corbett et al., 1998; Dulaiova et al., 2008) using sediments discharged from the subglacial environment. For these tests, four separate aliquots of sediment (50 g) from the proglacial river were incubated with Ra-free water in a sealed 1 L high-density polyethylene bottle for greater

than five half-lives (>20 days). Samples were flushed into a cold trap and scintillation cells using helium and analyzed in triplicate on alpha scintillation counters (Corbett et al., 1998). Wet sediment ^{222}Rn activities in dpm g^{-1} were converted to pore water ^{222}Rn activities (dpm L^{-1}) using wet bulk densities and porosities (Supplementary Material).

Radon-222 diffusion from sediments in subglacial channels was another potential source of ^{222}Rn beneath the GrIS. We employed a laboratory method described by Chanyotha et al. (2014) to quantify the diffusive flux. Briefly, 100 g of wet subglacial sediment and 500 mL of ^{222}Rn-free water were sealed inside a gas tight reaction flask connected in a closed loop with a RAD7. Air was pumped through a gas diffusion stone immersed in the water phase using the built in RAD7 pump, then through the desiccant, and back to the radon analyzer where the activity was measured and recorded. While gas leakage is not an issue for routine measurements, a known small leak within the internal air pump of the RAD7 was corrected during the multi-day experiment according to the approach described in Chanyotha et al. (2014). The diffusive flux was determined from the near-linear slope of ^{222}Rn activity in the reaction flask versus time over the first several hours of the experiment. Slope uncertainty was used to estimate the uncertainty of the diffusive flux.

Leakage is an issue for this approach, not necessarily from diffusion through the walls of the plastic bottle but from a known small leak in the internal air pump of the RAD7 as described in Chanyotha et al. (2014). This is not an issue for routine measurements with the RAD7, but needs to be corrected for in the multi-day sediment equilibration method. The data has been leak corrected according to the approach described in Chanyotha et al. (2014)

3 Results

3.1 Discharge

Warmer average air temperatures resulted in nearly twice as much annual discharge in 2012 as in 2011, corresponding to ~2.4 and 1.4 km^3, respectively within the Leverett Glacier catchment (Figure 2). Average flows of the proglacial river in the summer were ~200 $m^3 s^{-1}$ in 2011 (Sole et al., 2013) and ~400 $m^3 s^{-1}$ in 2012 (Tedstone et al., 2013). In 2012, the largest melting event since at least 1889, as indicated by ice cores at the Summit Station, occurred on July 12th (day 194) when over 98% of the surface of the GrIS experienced melting (Nghiem et al., 2012). During this period, river discharge reached ~800 $m^3 s^{-1}$ (Tedstone et al., 2013), almost three times larger than maximum discharge in 2011 (Figure 2; Sole et al., 2013). Furthermore, in 2011 the river was largely ice-covered until day 160, while in 2012 the river was ice free from the start of sampling (day 133) onward.

3.2 EC and SSC

We used EC as a proxy for the concentration of dissolved solutes in the proglacial river. During both 2011 and 2012, EC was elevated in the early season (60-100 µS cm^{-1}) and decreased to 10-20 µS cm^{-1} with increasing river discharge (Figure 2; Butler, 2014; Hawkings et al., 2014). These results are consistent with the EC range reported in 2009 (Bartholomew et al., 2011). Butler (2014) and Hawkings et al. (2014) observed diurnal variations in EC through much of the 2011 and 2012 seasons, which in general were inverse to river discharge. During both seasons, peaks in EC punctuated the record.

The SSC varied between 1-7 g L^{-1} in 2011 (Butler, 2014) and 1-4 g L^{-1} in 2012 (Hawkings et al., 2014); these concentrations were similar to values reported for 2009 and 2010

(Cowton et al., 2012). Like EC, diurnal variations in SSC occurred throughout much of the 2011 and 2012 melt seasons, however, these diurnal variations in SSC generally increased with rising river discharge. In 2012, peaks in SSC and EC generally occurred simultaneously (Figure 2, dashed boxes) as noted by Hawkings et al. (2014) and in line with observations in 2009 (Bartholomew et al, 2009). In 2011, SSC and EC peaks were largely decoupled (Figure 2).

3.3 Radon-222 in the Proglacial River

In both 2011 and 2012, the highest ^{222}Rn activities were observed in the early season and generally decreased with increasing river discharge (Figure 2). In 2011, typical ^{222}Rn activities in the early season (days 132-160) were between 10-15 dpm L^{-1}. Following day 170, activities were generally between 2-5 dpm L^{-1}. In 2012, higher ^{222}Rn activities were observed in the early season, typically between 5-18 dpm L^{-1}, falling to between 2-10 dpm L^{-1} after day 150. In a small proglacial river ~100 km north of our field site, Bhatia et al. (2011) reported significantly higher ^{222}Rn activities (25-76 dpm L^{-1}), though peak river discharge rates (~2 m^3 s^{-1}) were orders of magnitude lower than at Leverett Glacier. Regardless, activities measured in this study and in Bhatia et al. (2011) are much higher than those generally observed in non-glaciated river catchments. For example, both Cook et al. (2003) and McCallum et al. (2012) report maximum ^{222}Rn activities of ~1 dpm L^{-1} in tropical and temperate rivers.

Significant peaks in ^{222}Rn are highlighted in Figure 2 by grey shaded boxes. In 2011, ^{222}Rn peaked at ~75 dpm L^{-1} in the early season (days 148-150); during this time, the river was ice covered and a small upwelling spring appeared at the glacier portal through which nearly all river discharge originated. A second large peak (days 190-200) was observed in ^{222}Rn when activities climbed to ~15 dpm L^{-1} from a pre-peak baseline of 3 dpm L^{-1} over a ~5 day period

(Figure 2). In 2012, ^{222}Rn peaks occurred regularly, approximately once every 8-10 days throughout the season (Figure 2). Radon-222 peaks in 2012 generally increased on the falling limb or inflection point of the hydrograph and decreased when river discharge rose (Figure 2). This general relationship between discharge and ^{222}Rn was not observed in 2011. In both field seasons, ^{222}Rn did not correlate with SSC or EC.

3.4 Radon activity in distributed system meltwater

Laboratory derived distributed system ^{222}Rn activities (Rn_{dis}) were estimated using the ^{222}Rn activity of porewater in sediments collected from the proglacial river (Section 2.4) and sediment properties (Corbett et al., 1998) including bulk density (ρ_B) and porosity (ϕ; Supplementary Material). Wet sediment ^{222}Rn activities (Rn_{sed}) were 0.064-0.093 dpm g^{-1} (avg=0.076 dpm g^{-1}, n=4). ρ_B and ϕ were identical for the three glacial river sediment samples analyzed and were 1.7 g cm^{-3} and 0.37 respectively. Our results are consistent with those of Dow et al. (2013), who estimated subglacial sediment ϕ in the Leverett Glacier catchment between 0.3-0.4. Using Equation 1 and assuming that subglacial sediment ϕ varied between 0.3-0.4, that Rn_{sed} was between 0.064-0.093 dpm g^{-1}, and that ρ_B=1.7 g cm^{-3}, Rn_{dis} would be expected to span from 270-530 dpm L^{-1}.

$$Rn_{dis} = \frac{Rn_{sed} \times \rho_B}{\phi} \times 1000 (g\ L^{-1}) \quad (1)$$

These values are lower than laboratory derived pore water ^{222}Rn activities in proglacial sediments reported by Bhatia et al. (2011), which were between 1285-3045 dpm L^{-1}. A number of factors could explain the difference between the two sites: including sediment grain size

253 (higher surface area/volume), degree of weathering (affects sediment ^{226}Ra parent activities), or
254 ^{238}U content of the sediment (Dulaiova et al., 2008).
255
256 **4 Discussion**
257 *4.1 Radon-222 sources and sinks*
258 Radon-222 has been used as a tracer of sediment pore water-surface water exchange
259 processes in a diverse range of environmental systems including rivers (McCallum et al., 2012),
260 the coastal ocean (Burnett and Dulaiova, 2003; Dulaiova et al., 2008), and in small glacier
261 catchments (Kies et al., 2010; Bhatia et al., 2011; Kies et al., 2015). In the following discussion,
262 we explore the utility of ^{222}Rn in tracing and quantifying meltwater fluxes from the subglacial
263 distributed system at a large Greenland outlet glacier, Leverett Glacier. There are a number of
264 sources and sinks capable of modulating ^{222}Rn activities in a proglacial river. We use a mass
265 balance approach, similar to those employed in studies of submarine groundwater discharge to
266 the coastal ocean (Burnett and Dulaiova, 2003; Dulaiova et al., 2008), in order to quantify the
267 sources and sinks for ^{222}Rn in the proglacial river (Figure 3):
268
269 $$J_{riv} = J_{dis} + J_{cha} + P_{SSL} + \lambda^{226}Ra - J_{atm} - \lambda^{222}Rn \quad (2)$$
270
271 Sources of ^{222}Rn include production from ^{226}Ra associated with suspended sediments (P_{SSL}),
272 production of ^{222}Rn through the decay of dissolved ^{226}Ra ($\lambda^{226}Ra$ where λ is the decay constant
273 for ^{222}Rn), ^{222}Rn diffusion through subglacial channel sediments (J_{cha}), and distributed system
274 meltwater (J_{dis}). Radon-222 sinks include radioactive decay ($\lambda^{222}Rn$) and atmospheric evasion
275 across the water/air interface (J_{atm}). Finally, J_{riv} is the ^{222}Rn flux (dpm s^{-1}) exported to the

glacier's front via the proglacial river and is derived by combining our continuous ^{222}Rn measurements (dpm m^{-3}) with the discharge record (m^3 s^{-1}). All source/sink terms can be directly evaluated except for J_{dis}; hence we use the "flux by difference" approach (Charette et al., 2008), which assumes that the unaccounted for ^{222}Rn in the mass balance model must be due to distributed system meltwater *(J_{dis})*. We discuss and evaluate each source and sink term for Equation 2 in the following sections. To provide context for the various source and sink terms below, note that J_{riv} ranged from 3.4-4.2×10^6 dpm s^{-1} and 7.2×10^3-3.4×10^6 dpm s^{-1}, for 2011 and 2012, respectively.

4.1.1 Suspended sediment ^{226}Ra (P_{SSL})

Suspended sediments are a potential source of ^{222}Rn to the river through decay of sediment bound ^{226}Ra. From the laboratory equilibration experiments described above (Section 2.4) we determined that the surface-bound ^{222}Rn activity of sediments at secular equilibrium is 0.076 dpm g^{-1} (Section 3.4). To calculate P_{SSL}, we first assume that suspended sediments could produce ^{222}Rn for 1-18 hours, the range of transit times observed for surface meltwater traveling through channelized drainage in the Leverett Glacier catchment (Chandler et al., 2013; Chandler et al., submitted). Coupling this result with SSC measurements, and assuming that bedload contributed an additional 30-60% of sediment (Cowton et al., 2012), we estimated the upper and lower bounds of the contribution from P_{SSL} to J_{riv}. Over the course of each melt season, P_{SSL} supplied between ~100 and 2.1×10^4 dpm s^{-1} ^{222}Rn in 2012 and ~100 and 2.4 ×10^4 dpm s^{-1} ^{222}Rn in 2011. On average, the upper limit of our P_{SSL} estimate contributed on average ~1% of J_{riv} in 2011 and 2012, respectively (Figure 4).

299 *4.1.2 Dissolved ^{226}Ra ($\lambda^{226}Ra$)*

300 The proglacial river also carried dissolved ^{226}Ra, which could have supported ^{222}Rn via
301 its decay. We observed ^{226}Ra activities of 0.02-0.09 dpm L^{-1} (avg 0.04 dpm L^{-1}, n=21) in the
302 proglacial river, with higher values in the early season and lower values in the late season. To
303 solve Equation 2 for J_{dis}, we used the average ^{226}Ra activity measured in the proglacial river.
304 Based on these results, ^{226}Ra decay supplies ~400 dpm s^{-1} when river discharge was 10 m^3 s^{-1}
305 and up to 3.2×10^4 dpm s^{-1} during the maximum river discharge observed in 2012. On average
306 during the 2011 and 2012 field seasons, dissolved ^{226}Ra supplies ~1% of J_{riv} (Figure 4).
307
308 *4.1.3 Diffusive flux of ^{222}Rn in channels (J_{cha})*

309 The diffusive flux of ^{222}Rn from channel floor sediments (subglacial or proglacial) is a
310 potential source of ^{222}Rn, particularly after the onset of widespread melting across the catchment
311 and development of a channelized system. Our laboratory sediment diffusion experiment yielded
312 a diffusive flux of 0.006 ± 0.002 dpm m^{-2} s^{-1} ^{222}Rn from glacial sediments. We use this result and
313 an estimate of channel floor area during peak river discharge to quantify the potential upper limit
314 of J_{cha}. To calculate channel floor area, we assume that all discharge moved through semi-
315 circular channels, that channels extended to 41 km from the ice margin (Chandler et al., 2013),
316 that the average number of channels per km catchment width was four (Schoof, 2010; Werder et
317 al., 2013), and that channel density linearly tapered to zero between the ice sheet margin and 41
318 km. Furthermore, we assumed that catchment width averaged 40 km (Bartholomew et al., 2011)
319 and that water moved through channels at 3 m s^{-1} (Cowton et al., 2013). Using these constraints,
320 we calculated a channel floor area of 2.75 km^2 during peak river discharge in 2012 and 1.5 km^2
321 during peak river discharge in 2011. This estimate amounts to 0.3-0.5% of the glacier's

322 catchment area, which is consistent with models of the channelized system (Schoof, 2010;
323 Werder et al., 2013). Using these estimates of channel floor area, J_{cha} supplied ~6×10^3-1.2×10^4
324 dpm s^{-1} ^{222}Rn in 2011 and 1.1×10^4-2.2×10^4 dpm s^{-1} ^{222}Rn in 2012. Finally, we assume that J_{cha} is
325 only important after river discharge surpasses 100 m^3 s^{-1} as before this time the channelized
326 system is undeveloped (Cowton et al., 2013), and hence, ^{222}Rn diffusion through channel floors
327 is negligible. Based on these estimates, J_{cha} could account for no more than <1-10% of J_{riv} in
328 2011 and 2012 (Figure 4).
329
330 *4.1.4 Gas exchange (J_{atm})*
331 The degassing of ^{222}Rn out of water is a function of molecular diffusion produced by the
332 activity gradient at the water/air interface as well as turbulent transfer, which is governed by
333 physical processes such as wind speed, current velocity, and topography. $J_{atm,}$ which we define
334 as the area-normalized flux of ^{222}Rn across the river/air boundary, can be written as:
335
336 $$J_{atm}=k(C_w-\alpha C_{atm}) \quad (3)$$
337
338 where C_w is the ^{222}Rn activity of water, C_{atm} is the ^{222}Rn activity in air (assumed here to be
339 negligible relative to the water activity), α is Ostwald's solubility constant and k is the gas
340 transfer velocity. The gas transfer velocity is dependent on kinematic viscosity, molecular
341 diffusion, and turbulence and is determined based on empirical relationships observed in
342 different environments for different gases. Borges et al. (2004) suggested that the gas transfer
343 velocity k should be in the range of 3-7 cm hr^{-1} while Dulaiova and Burnett (2006) calculated a
344 gas transfer velocity for ^{222}Rn up to 10 cm hr^{-1} in moving water and high winds.

345 Because of occasional strong winds and a river current of ~1-3 m s^{-1} (Cowton et al.,
346 2013), we chose a constant, upper limit k of 12 cm hr^{-1} for the duration of the time series. With
347 these assumptions, J_{atm} varied between <0.01-0.7 dpm m^{-2} s^{-1} in 2011 and 0.03-0.6 dpm m^{-2} s^{-1} in
348 2012. Scaling these area normalized J_{atm} values to total J_{atm} requires an estimate of river surface
349 area (1100-6000 m^2) between the ice terminus and the sampling site. From this surface area we
350 determined that J_{atm} was in the range of 800-4,000 dpm s^{-1} ^{222}Rn, which was <1% of J_{riv} on
351 average. The negligible effect of gas loss suggested by these calculations is supported by discrete
352 ^{222}Rn samples collected at the glacier's terminus, which were within error of the continuous
353 measurements made 1 km downstream (Figure S1; Supplementary Material).
354 These estimates do not account for any potential loss of ^{222}Rn into the headspace of
355 subglacial air-filled cavities. However, if these environments are largely closed systems, ^{222}Rn
356 build up in the headspace would reduce the water-air concentration gradient and therefore
357 minimize the ^{222}Rn loss from the water phase. While there is evidence for open system channels
358 at the ice bed within several km from the ice margin (Chandler et al., 2013), subglacial gas loss
359 is likely much smaller than in the proglacial river. Air-filled subglacial channels far from the ice
360 sheet margin will only exist during the falling limb of the hydrograph following substantial
361 surface meltwater inputs and channel expansion. These cavities will close within hours to days of
362 opening because of glacial creep (Meierbachtol et al., 2013). If large quantities of ^{222}Rn were lost
363 to air-filled cavities, then ^{222}Rn activities would decrease on the falling limb of the hydrograph
364 yet we generally observed the opposite trend in 2012 (Figures 2). Based on our calculations and
365 field measurements (Supplementary Material), we determined that J_{atm} was negligible in our
366 calculation of J_{dis}.
367

368 4.1.5 *Radon-222 decay ($\lambda^{222}Rn$)*

369 When distributed system meltwater discharges into the channelized system far from the
370 ice margin, some fraction of ^{222}Rn will decay before reaching the ice terminus. For example,
371 during a typical 7 hour transit through the channelized system of Leverett Glacier in July
372 (Cowton et al., 2013), ~5% of unsupported ^{222}Rn will decay. During the early melt season, when
373 the snow line is at a low elevation and river discharge is <10 m^3 s^{-1}, meltwater transit times in
374 channelized drainage are likely no more than 3 hours as water takes a more direct route to the
375 margin (Chandler et al., 2013; Cowton et al., 2013). In this case, 2% of the unsupported ^{222}Rn
376 decays in the channelized system before reaching the ice margin. By the peak melt season, tracer
377 experiments indicate that transit times in the channelized drainage system are 10-24 hours
378 (Chandler et al., (submitted) since the catchment extends upwards of ~80 km from the margin
379 and subglacial flow paths are more convoluted. As the location of these experiments was likely
380 near the upper limit of channelized drainage in the catchment (Chandler et al., 2013), we assume
381 nearly all meltwater traveling via channelized drainage reaches the ice sheet margin in <24
382 hours. Hence for our model, we assume meltwater moving through the channelized system has a
383 transit time between 1 and 24 hours representing a <1-17% loss of ^{222}Rn.
384
385 *4.2 Quantifying the distributed system flux*

386 After rearranging Equation 2, we solved for the upper and lower bounds of J_{dis} (Figure 5).
387

388 $$J_{dis} = J_{riv} - J_{cha} - P_{SSL} - \lambda^{226}Ra + \lambda^{222}Rn \quad (4)$$

389

To calculate the likely range of J_{dis}, we propagated the uncertainty of each ^{222}Rn source and sink. The largest source of uncertainty in J_{dis} came from the ^{222}Rn and river discharge measurements used to calculate J_{riv}.

With the exception of days 200-202 in 2011 when J_{riv} dropped to near zero, non-distributed system ^{222}Rn sources cannot account for the vast majority of J_{riv} (Figure 4), we conclude that J_{dis} must contribute the bulk of the ^{222}Rn flux in the proglacial river. Furthermore, ^{222}Rn decay during subglacial transit through the channelized system ($\lambda^{222}Rn$) and gas loss to the atmosphere (J_{atm}), did not significantly impact the timing or flux of J_{riv}. Given that J_{dis} dominates the ^{222}Rn mass balance for the Leverett Glacier proglacial river, we conclude that ^{222}Rn can be used as a passive tracer of distributed system flows to the ice margin at this field site. This approach should be applicable to other settings, though an essential requirement is subglacial hydrological systems that discharge into a single proglacial river, which permits the quantification of J_{riv}, the main term in the model.

The distributed system meltwater flux (Q_{dis}) can be calculated if J_{dis} and the ^{222}Rn activity of distributed system meltwater (Rn_{dis}) are known:

$$Q_{dis} = J_{dis}/Rn_{dis} \quad (5)$$

This approach assumes that distributed system meltwaters originate from material similar to the proglacial sediments we used to estimate Rn_{dis} (Sections 2.4 and 3.4), and that the transit time of distributed system meltwaters are >20 days (Niu et al., 2015). If the transit time is shorter, Rn_{dis} would decrease and the Q_{dis} fluxes below would increase proportionately.

If the ^{222}Rn activities in distributed system sediments are 270-530 dpm L^{-1} (Sections 2.4 and 3.4), then Q_{dis} would vary between <0.1 to 17 m^3 s^{-1} and <0.1 to 14 m^3 s^{-1} over the course of the 2011 and 2012 melt seasons, respectively. As a fraction of total river discharge in 2011, Q_{dis} peaked at ~22% in the early season when river discharge was ~1 m^3 s^{-1} and reached a minimum of <0.1% between days 202-204. In 2012, Q_{dis} was between 3-5% (0.1-0.5 m^3 s^{-1}) of total river flow in the early season (days 130-150) and 1-4% (0.1-33 m^3 s^{-1}) following day 150. The weighted mean of Q_{dis} relative to total river discharge was between 1-2.4% (0.35-8.5 m^3 s^{-1}) in 2011 and 0.7-1.6% (<1-12.8 m^3 s^{-1}) in 2012. However, since we were not able to obtain samples of distributed system water directly via borehole sampling (Tranter et al., 1997; Andrews et al., 2014), these estimates of Q_{dis} carry significant uncertainty; therefore, we will use J_{dis} for determining the timing and relative magnitude of distributed system fluxes.

4.3 Seasonal and interannual variability in the distributed system flux

Channels at the ice sheet bed are zones of low-pressure relative to the surrounding distributed system (Röthlisberger, 1969) and generally act to scavenge distributed system meltwater (Boulton et al., 2009). However, during large surface runoff events, such as supraglacial lake drainages or periods of rapid warming, channels may be overwhelmed forcing water into the distributed system (Bartholomew et al., 2012; Gulley et al., 2012). Once surface meltwater runoff decreases, water pressure in channels falls and the flux of distributed system drainage to the ice sheet margin surges (Hubbard et al., 1995; Boulton et al., 2009). This process has been hypothesized to result in more connectivity between channelized and distributed systems causing an overall increase in the spatial extent of subglacial drainage (Andrews et al., 2014). This in turn may lead to less water volume at the ice sheet bed and could explain observed

435 mid-late summer slowing of land-terminating sections of the GrIS (Sole et al., 2013). Hence, the
436 mechanisms that control the characteristics of distributed system drainage likely play a key roll
437 in modulating the speed of GrIS outlet glaciers, especially because distributed system networks
438 make up by far the largest portion of the ice sheet bed area.

439 In 2011, the largest multiday peak in J_{dis} (Figure 5) (days 190-200) occurred during the
440 onset of melting and ice acceleration (Sole et al., 2013) at high elevations (>1400 m) within the
441 catchment, and the expansion of the channelized system to at least 40 km from the ice sheet
442 margin (Chandler et al., 2013). During the 2012 time series, there were four major multiday
443 peaks in J_{dis} (Figure 5). The largest 2012 peak occurred on the falling limb of the hydrograph of
444 the widely publicized extreme melting event (Nghiem et al., 2012) during which river discharge
445 reached ~800 m^3 s^{-1} (day 196; Figure 5). These results provide direct evidence that drainage of
446 distributed regions follows periods of channelized system expansion due to rapid increases in
447 surface meltwater runoff. Following the largest peaks in J_{dis} in 2011 and 2012, significant diurnal
448 variations were observed in J_{dis} (days 205-210 in 2011 and days 199-205 in 2012; Figure 6).
449 These daily cycles in J_{dis} suggest a high degree of connectivity between the distributed and
450 channelized systems with increases in flux from the distributed on the falling limb of the
451 hydrograph when subglacial water pressure subsides (Figure 6).

452 Bartholomew et al. (2011) and Butler (2014) found evidence that SSC/EC peaks at
453 Leverett Glacier are triggered by supraglacial lake drainage events. These events likely increase
454 the connectivity of the channelized system (Bartholomew et al., 2011a), and may lead to the
455 expulsion of distributed system meltwater. In general, peaks in J_{dis} were not correlated with
456 SSC/EC peaks, nor did peaks in SSC/EC lead to enhanced ^{222}Rn concentrations (Figure 2). Lake
457 drainage events clearly increase the suspended sediment load which may lead to post mixing

458 solute acquisition reactions, causing meltwaters to rapidly acquire dissolved solutes (Raiswell,
459 1984; Tranter et al., 1993). Conversely, ^{222}Rn equilibrium in the distributed system will likely be
460 reached long before subglacial meltwaters become saturated with respect to weathering minerals.
461 Hence, we would expect more variation in solute concentrations (EC) in the distributed system
462 than ^{222}Rn activities. Consequently, lake drainage events could produce the observed SSC/EC
463 peaks without a corresponding J_{dis} peak if they act to flush small volumes of distributed system
464 meltwater with high solute concentrations to the ice sheet margin.
465

466 **5 Conclusions**

467 Using a mass balance model for ^{222}Rn in a large glacial catchment of the GrIS, we found
468 that on average, >90% of the ^{222}Rn in the proglacial river is sourced from the subglacial
469 distributed system. Hence, at Leverett Glacier, ^{222}Rn acts as a conservative, passive tracer of
470 distributed system meltwater fluxes. These fluxes varied on diurnal, seasonal, and interannual
471 time scales. Based on ^{222}Rn measurements, large peaks in distributed system drainage appear to
472 be initiated by the expansion of the channelized system into presumably distributed regions of
473 the ice sheet bed and by rapid increases in supraglacial meltwater runoff. During a large multiday
474 J_{dis} peak in 2011 (days 190-200; Figure 5), SF_6 tracer experiments (Chandler et al., 2013) and ice
475 acceleration (Sole et al., 2013) suggested the channelized network expanded coincident with the
476 J_{dis} peak. In 2012, four major multiday J_{dis} peaks were observed (Figure 5), the biggest of which
477 occurred on the falling limb of the hydrograph during the largest surface meltwater runoff event
478 observed in Greenland since at least 1889 (days 196; Nghiem et al., 2012). These results imply
479 that rapid warming events, which initially cause short term glacial acceleration (Tedstone et al.,
480 2013), may lead to enhanced distributed system drainage, a process which could lessen the total

481 water volume at the ice sheet bed and ultimately, explain the observed mid-summer ice sheet
482 slowing at Leverett Glacier (Sole et al., 2013; Tedstone et al., 2013). Following the largest peaks
483 in J_{dis} in 2011 and 2012, significant diurnal variations were observed in J_{dis}, indicative of a
484 highly connected distributed system whereby the distributed system water flux substantially
485 increases at night when channelized system water pressure subsides.
486 Based on our laboratory-based sediment equilibration measurements of ^{222}Rn activities in
487 distributed system fluids, we estimate that distributed system meltwater fluxes vary seasonally
488 and are on the order of 1-5% of river discharge. The weighted mean Q_{dis} relative to total river
489 discharge was between 1-2.4% in 2011 and 0.7-1.6% in 2012. Future studies should endeavor to
490 collect samples for ^{222}Rn analysis directly from distributed and channelized systems so as to
491 better constrain Q_{dis}. Furthermore, utilizing continuous ^{222}Rn measurements provides a practical
492 tool to capture hourly variations in ^{222}Rn activity as well as episodic events that might otherwise
493 be missed if solely relying on discrete ^{222}Rn measurements. Additionally, the detection limit and
494 measurement uncertainty using the water probe extraction method (Section 2.3) is much lower
495 than discrete sampling (Supplementary Material, Figure S1). Our results demonstrate that there is
496 great potential for continuous ^{222}Rn measurements in proglacial rivers to aid our understanding
497 of how distributed system fluxes impact glacial hydrology, ice-dynamics, and biogeochemical
498 fluxes.
499
500
501 **Acknowledgements**
502 We acknowledge and thank our funding sources: U.S. National Science Foundation Arctic
503 Natural Sciences Program (ANS-1256669); Woods Hole Oceanographic Institution Arctic

Research Initiative, Ocean Ventures Fund, and Ocean Climate Change Institute; United Kingdom Natural Environment Research Council studentship (NE/152830X/1); the Carnegie Trust, Edinburgh University Development Trust. We also thank the Leverett field camp members who helped with data collection especially Catie Butler for collecting the 2011 electrical conductivity data that appears in this work. Data presented in this study is archived at: www.aoncadis.org/dataset/GrIS_RADON.html. Finally, we thank the Editor Derek Vance and three anonymous reviewers whose suggestions significantly improved this manuscript.

512

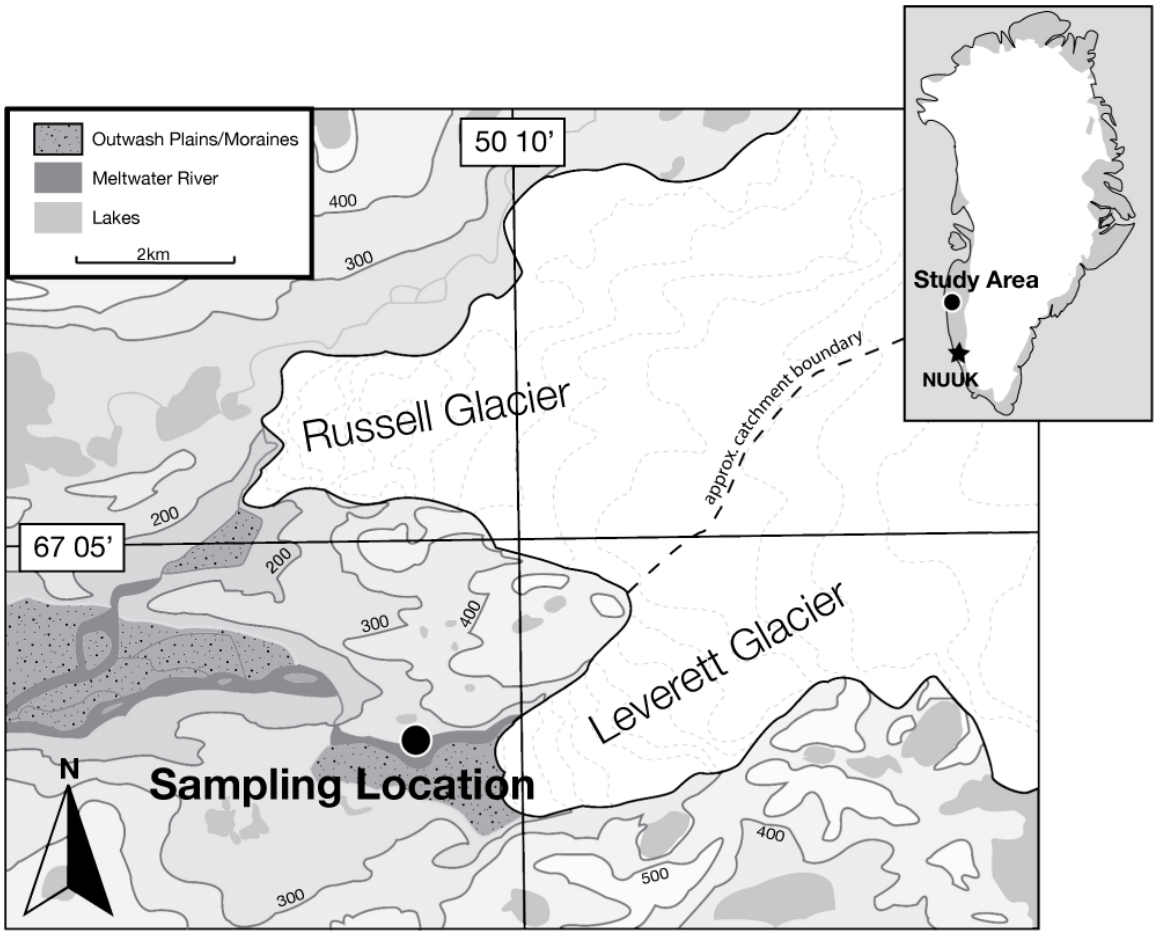

513

514

515 Figure 1: Location of Leverett Glacier in west Greenland. The primary sampling location for
516 continuous ^{222}Rn measurements is indicated by the black circle though some early season
517 deployments of the ^{222}Rn sensor occurred much closer to the glacier terminus. Figure adapted
518 from Hawkings et al. (2014).

519

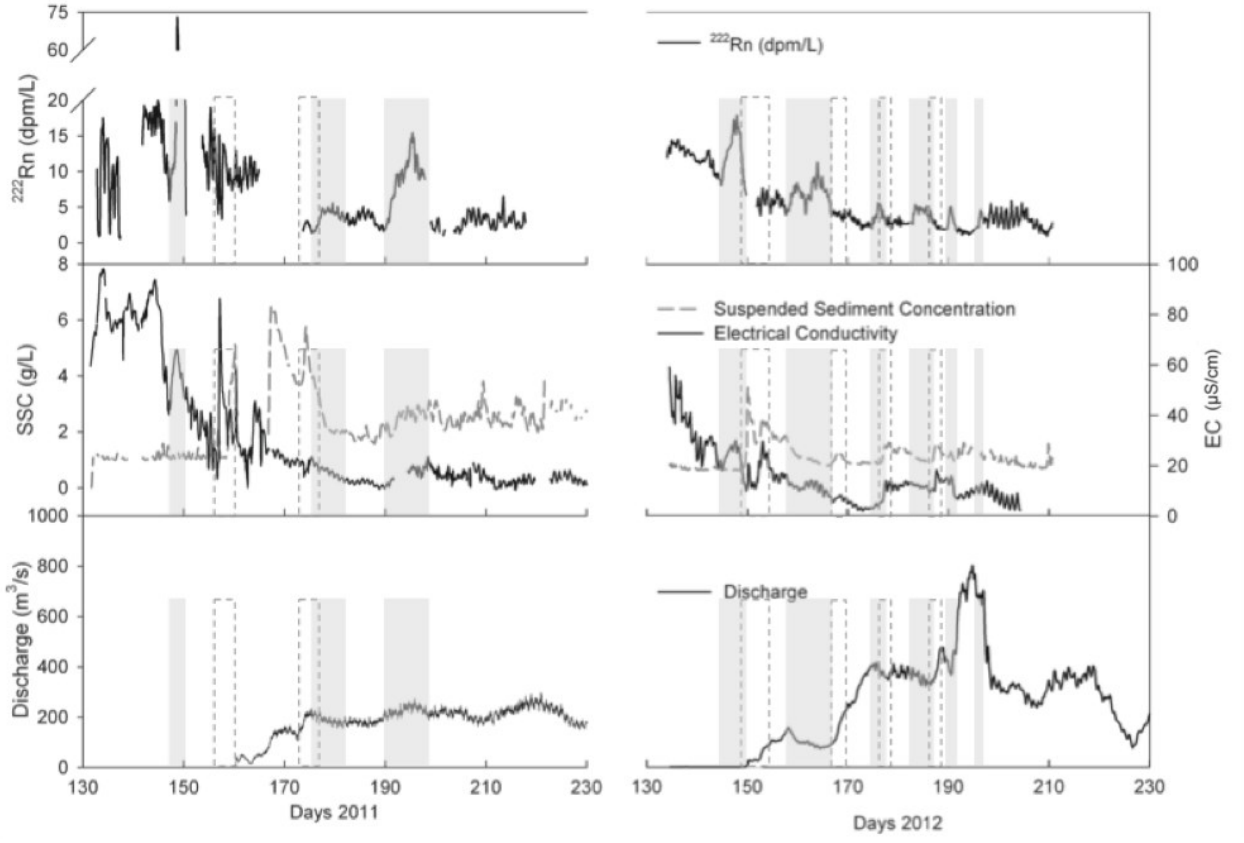

Figure 2: Results from 2011 and 2012 field seasons. Top panels: radon-222 activity (dpm L^{-1}); middle panels: EC and SSC (Hawkings et al., 2014); bottom panels: river discharge (Sole et al., 2013; Tedstone et al., 2013). Shaded grey boxes represent ^{222}Rn peaks while dashed grey boxes are SSC/EC peaks, which likely correspond to supraglacial lake drainage events (discussed in text).

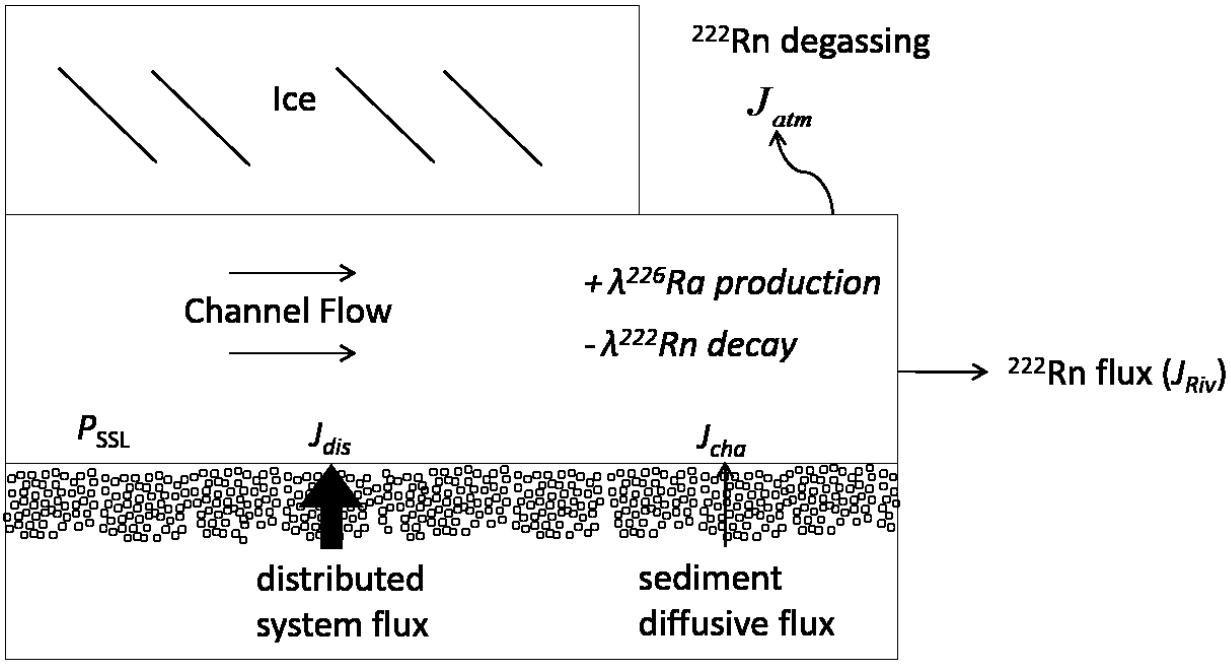

Figure 3: Summary of ^{222}Rn sources and sinks in the proglacial river. Sources of ^{222}Rn include the distributed system flux (J_{dis}), ^{222}Rn diffusion through sediments into channels and cavities (J_{cha}), ^{226}Ra bound to the surface of the suspended sediment load (P_{SSL}), and the decay of dissolved ^{226}Ra ($\lambda^{226}Ra$). The sinks of ^{222}Rn include gas loss to the atmosphere (J_{atm}) and radioactive decay of ^{222}Rn ($\lambda^{222}Rn$). The flux of ^{222}Rn from the river (J_{riv}) is the summation of these variables.

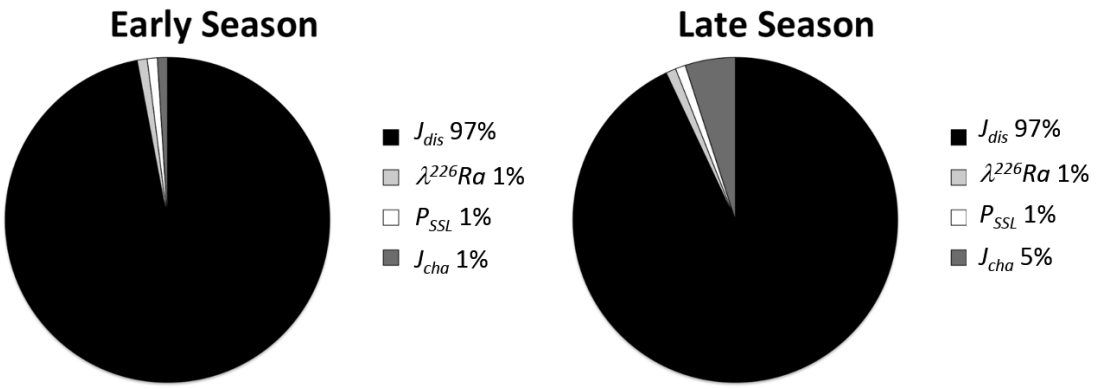

Figure 4: Average contributions from 2011 and 2012 of ^{222}Rn sources to J_{riv} in the early melt season (river discharge <100 m^3 s^{-1}) and during the late melt season (river discharge >100 m^3 s^{-1}). Our mass-balance model suggests that throughout the melt season, the bulk of ^{222}Rn in the proglacial river is derived from the distributed system. Model calculations suggested that the ^{222}Rn contribution from P_{SSL}, $\lambda^{226}Ra$, *and* J_{cha} were often <<1% of the total J_{riv}; in these instances, for the purpose of clarity in this figure, they have been rounded to their upper limit estimates (1%).

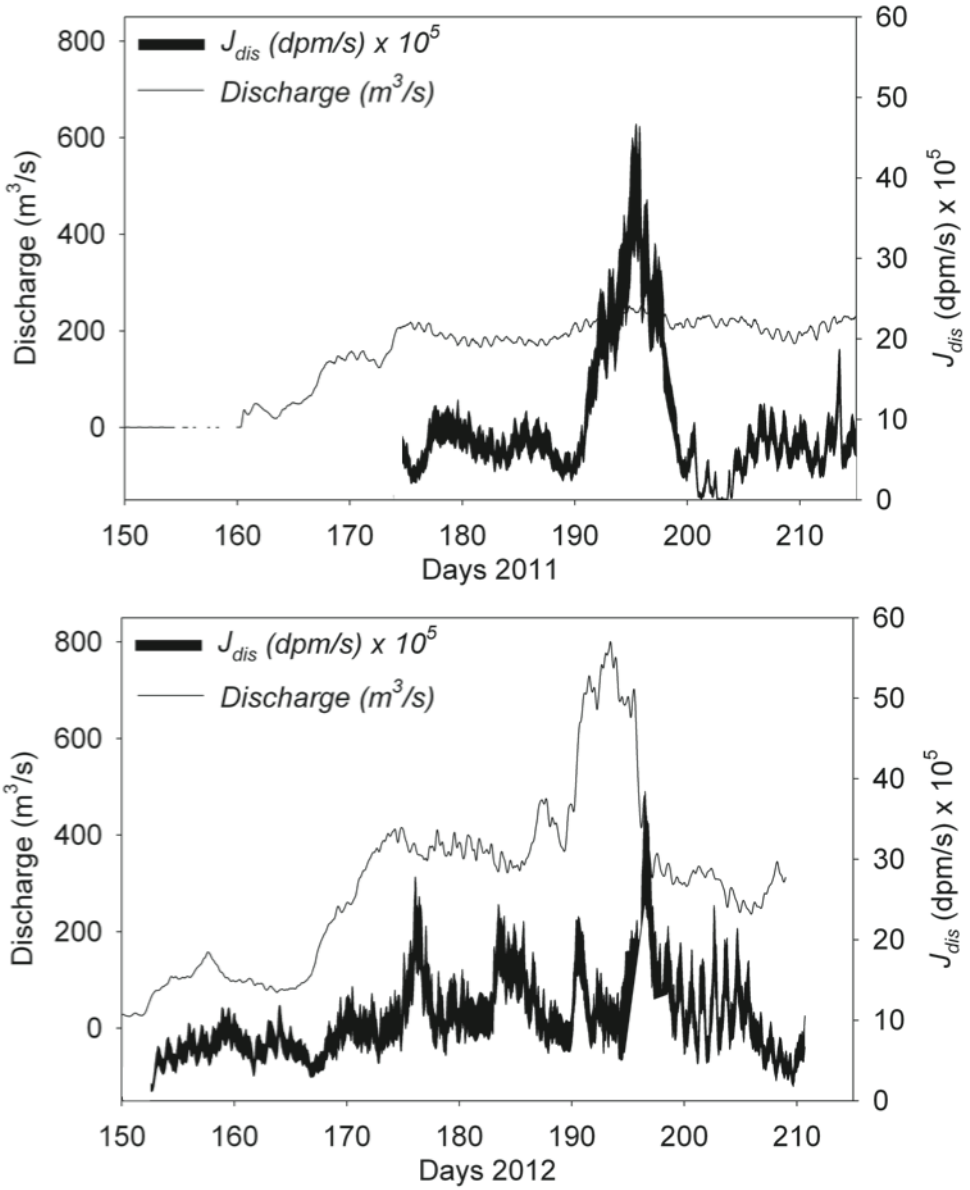

548

549 Figure 5: The estimated subglacial distributed system flux (J_{dis}) from Leverett Glacier and
550 discharge of the proglacial river in 2011 and 2012 (black line). The width of J_{dis} represents
551 uncertainty in this parameter (see text).

552

553

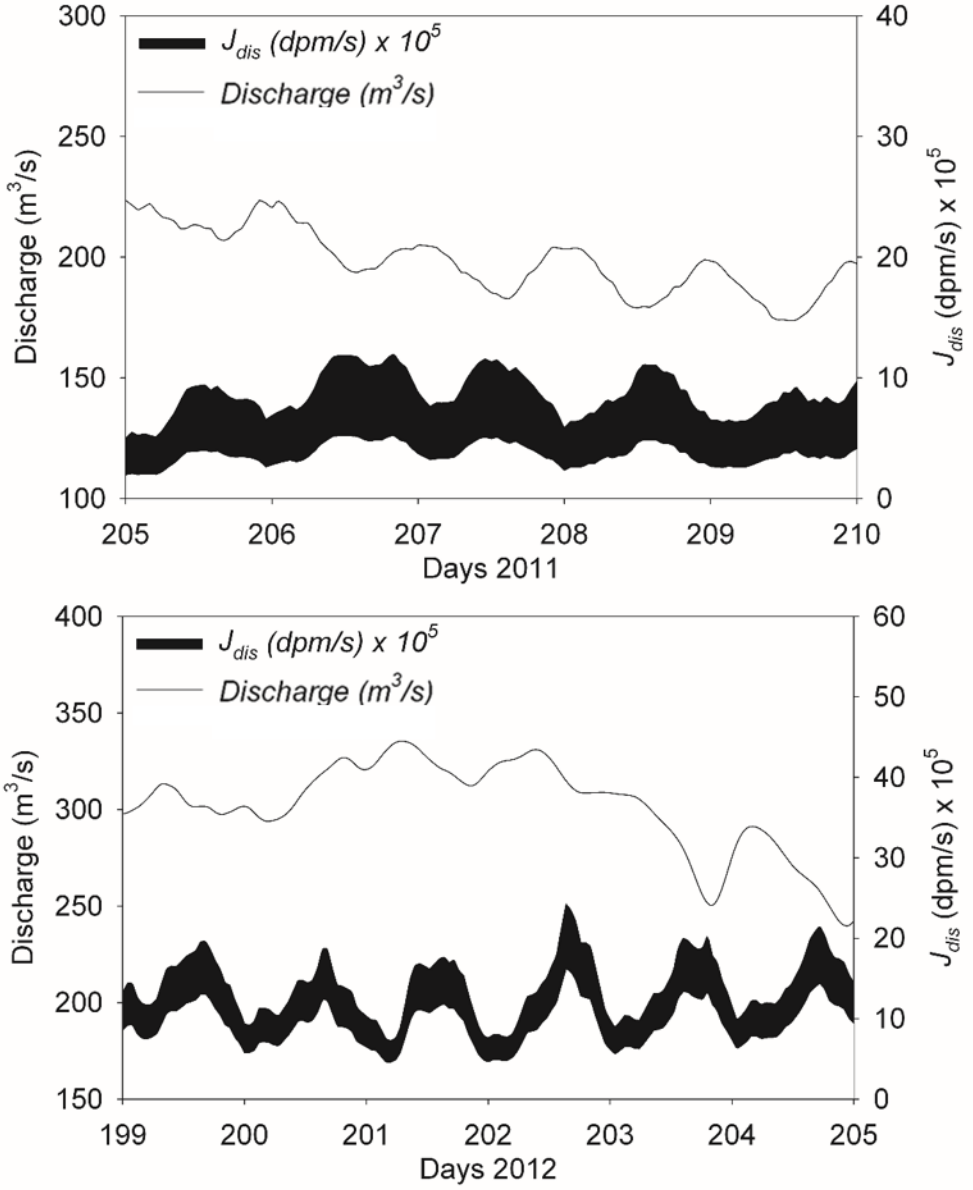

554

555 Figure 6: Diurnal variations in J_{dis} occurred in both the 2011 and 2012 melt seasons. In general,

556 J_{dis} peaks occurred on the falling limb of the hydrograph. We hypothesize that during this period,

557 distributed system meltwater was drawn into the channelized system as water pressure dropped
558 in subglacial channels.

559 **Supplementary Material**

560 *S1 Water probe response time*

561 During the 2011 and 2012 field seasons, several factors related to the water probe
562 setup may have influenced the response time of the water probe. First, in order to keep
563 the RAD7 a safe distance from the unstable riverbank, the length of tubing between the
564 detector and water probe had to be increased (from 8 to 12.5 m) effectively changing the
565 system air volume from 1650 to 1750 cm^3. Furthermore, the interface area of the
566 membrane coil changed as two Accruel® membrane coils of slightly different lengths (a
567 2.1 m coil and the 2.2 m coil within the Durridge Inc. 'water probe') were used
568 interchangeably across the two field seasons. The effect of these changes was quantified
569 using the empirical relationships developed by Shubert et al., (2012), which suggest that
570 our minor changes in air volume and membrane interface area likely only caused a 12-
571 minute difference in equilibration time. This is a negligible difference when considering
572 that the minimum time-scale over which significant changes in observed river ^{222}Rn were
573 diurnal. Furthermore, a field test was conducted in which both membrane coils were
574 simultaneously deployed in the proglacial river for 12 hours. During this test, both
575 systems recorded ^{222}Rn activities well within the statistical counting errors.
576 Consequently, the continuous ^{222}Rn record reported here is a compilation of results
577 obtained using both water probes. During deployment, the membrane coil was checked
578 daily for wear and sediment buildup on its surface. Throughout either field seasons, no
579 algae or sediment buildup was observed. To test the effectiveness of long term
580 deployment of the membrane coil over the course of a melt season, two probes were
581 deployed simultaneously, one that had been in continual use for ~30 days and a second

582 unit with a new membrane coil. Following an initial equilibration period, both units
583 measured identical ^{222}Rn activities (within the method's uncertainty) for several days.

584 To assess the water probe's response to changes in ^{222}Rn activity, we conducted
585 several laboratory experiments. First, the water probe was deployed simultaneously with
586 the more conventional air-water equilibrating spray chamber (Burnett and Dulaiova,
587 2003) in a 200 L tank of circulating 10˚C seawater for 70 hours. Seawater was
588 continuously pumped into the tank from Vineyard Sound, ~50 m offshore of Woods Hole
589 (MA). The air-water equilibrator spray chamber provided a baseline from which to
590 compare the water probe, because with an optimum setup, its equilibration time is less
591 than 30 minutes (Schubert et al., 2012). The residence time of seawater in the tank was
592 <1 hour and water was kept in constant motion using six submersible bilge pumps, each
593 capable of pumping ~30 L min^{-1}. Slow but significant changes in ^{222}Rn were observed by
594 both the spay chamber and water probe likely caused by the changing tide and submarine
595 groundwater discharge (Burnett and Dulaiova, 2003). The equilibration time was defined
596 as the length of time at which the recorded ^{222}Rn activities reached an activity plateau
597 within the statistical counting errors. With this experimental setup, the water probe
598 required an initial six-hour equilibration time while the spray chamber reached
599 equilibrium in <30 min. Subsequent changes in ^{222}Rn activity measured by the water
600 probe lagged 1-2 hours behind the spray chamber. In a separate experiment, the water
601 probe and spray chamber were allowed to equilibrate with ^{222}Rn-free water before being
602 moved quickly into a tank containing ^{222}Rn-enriched groundwater. In this case, both
603 water probe and spray chamber systems responded to the activity change in <30 minutes
604 though the water probe required much longer to reach the new equilibrium plateau.

605 To determine the equilibration time of the water probe system in the proglacial
606 river, we examined the first six hours of data recorded after the water probe was freshly
607 deployed (see Figure S2 for one example). Our analysis included 14 separate
608 deployments in 2011 and 2012 in river flows ranging from 1 to 750 $m^3 s^{-1}$. In each case,
609 an equilibration plateau was reached within two hours of deployment regardless of river
610 flow rate or system configuration (as described above). The equilibration time was
611 therefore three times faster than the laboratory experiments. This was likely because
612 water in the proglacial river was flowing much faster than in laboratory experiments
613 keeping the ^{222}Rn activity gradient at the water/air interface of the membrane coil closer
614 to 100%. These results support the findings of Hofmann et al. (2011) and Schubert et al.
615 (2012) showing that the water flow rate over the membrane coil is the most important
616 factor for passive ^{222}Rn extraction. Because of the much faster equilibration time in the
617 proglacial river, we expect the water probe's response time to changing ^{222}Rn activities
618 was also faster in the field than the one to two hours suggested by laboratory
619 experiments.

620 In summary, when interpreting results from continuous ^{222}Rn measurements, we
621 assume changes in ^{222}Rn activity recorded by our methods occurred within one hour of
622 actual ^{222}Rn activity changes in the proglacial river. Also, we have excluded ^{222}Rn results
623 from the first two hours from each fresh deployment while the water probe was
624 equilibrating.

625 *S2 Sediment Properties*

626 The porosity and bulk density of glacial flour collected in the proglacial river was

627 determined using the moisture content and particle density measured in the laboratory.
628 Moisture content (%M) was determined by weighing sediments before and after drying at
629 100˚C: using Equation S1:
630

$$\%M = \frac{wet\ \ wt. - dry\ wt.}{wet\ wt.} \square 100 \quad \text{(S1)}$$

631
632
633 Grain density (ρ_s) was determined using the oven dry weight and volume of sediment.
634 The volume of sediment was determined by adding the sediments to a volumetric flask
635 and measuring the weight of water displaced by the sediments.
636 Bulk density (β_D) was calculated using Equation S2
637

$$\beta_D = \frac{1}{\left(\left[\frac{1}{100 - \%M}\right] \times 100 + \frac{1}{\rho_z}\right) - 1} \quad \text{(S2)}$$

638
639 where ρ_s is the average sediment grain density of triplicate analysis. Finally, porosity (ϕ)
was estimated from Equation S3.
640

641 $$\phi = (\rho_s - \beta_D)/\rho_s \quad \text{(S3).}$$

642

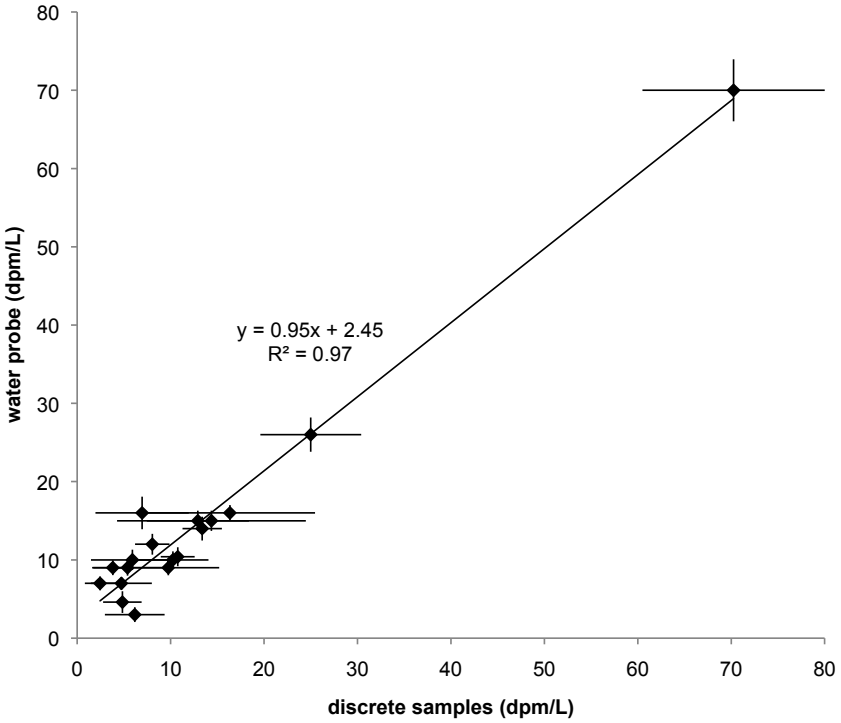

643

644 Figure S1: Comparison of discrete ^{222}Rn samples with comparable time-series
645 measurements using the water probe. Error bars represent 1-sigma counting errors on
646 each measurement. Many of these discrete ^{222}Rn samples were taken at the ice terminus
647 while the water probe measured ^{222}Rn downstream. This implies that gas loss in the
648 proglacial river between the ice terminus and the water probe was within the errors of our
649 measurements.

650

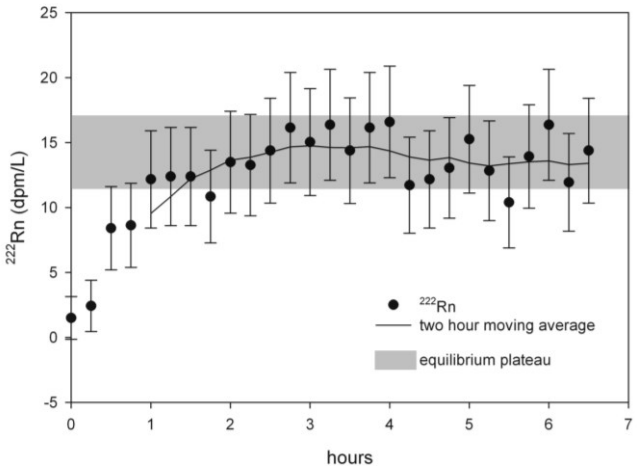

651

652 Figure S2: Equilibration time of the ^{222}Rn water probe on 6/2/2011 (day 153) after being
653 deployed in the proglacial river. Throughout the 2011 and 2012 field seasons, the water
654 probed required 1-2 hours to reach an equilibrium plateau, the time at which the recorded
655 radon activities reach an equilibrium activity plateau within the statistical counting errors.

656

Table S1. Summary of 250 mL discrete ^{222}Rn samples collected in the proglacial river in 2011.

Distance	Day	Date	^{222}Rn	+/-	EC
			dpm L^{-1}		µS cm^{-1}
0.5	128.5	5/8/11	15.9	6.4	
0.5	129.6	5/9/11	3.2	2.1	
0.5	132.5	5/12/11	3.2	2.8	69
0.5	132.5	5/12/11	7.0	5.4	69
0.5	132.8	5/12/11	4.3	3.0	75
0.5	132.8	5/12/11	5.9	4.4	75
0.5	133.4	5/13/11	4.8	2.1	94
0.5	133.4	5/13/11	7.0	6.4	94
0.5	133.7	5/13/11	18.2	10.1	79
0.5	133.7	5/13/11	14.5	7.5	89
0	133.6	5/13/11	4.3	3.9	
0	133.6	5/13/11	13.4	2.1	
0.5	134.5	5/14/11	9.1	2.1	90
0.5	134.5	5/14/11	7.0	4.4	90
0.5	135.5	5/15/11	5.4	2.8	74
0.5	135.5	5/15/11	7.0	6.2	76
0.5	136.0	5/16/11	10.8	1.8	81
0.5	137.5	5/17/11	9.1	6.2	76
0.5	137.5	5/17/11	1.6	2.0	76
0.5	139.6	5/19/11	4.3	1.8	81
0.5	140.8	5/20/11	5.9	1.1	73
0.5	140.8	5/20/11	5.4	2.8	73
0.5	141.6	5/21/11	14.0	4.1	75
0.5	145.8	5/25/11	4.3	4.7	65
0.5	144.6	5/24/11	6.9	3.2	88
0	147.7	5/27/11	67.4	11.6	49
0	147.7	5/27/11	32.2	7.3	45
0.5	147.8	5/27/11	7.5	2.8	45
0.5	147.8	5/27/11	12.9	3.0	45
0	148.5	5/28/11	41.4	8.1	85
0	148.5	5/28/11	54.3	7.3	84
0.5	148.5	5/28/11	70.3	9.7	62
0.5	149.8	5/29/11	24.3	6.2	40
0	149.8	5/29/11	17.8	8.8	40
0	151.9	5/31/11	17.8	3.1	37
0	148.8	5/28/11	6.5	3.5	61
0	150.8	5/30/11	5.4	1.3	40
0.5	150.8	5/30/11	14.7	6.8	40

659

Distance	Day	Date	^{222}Rn	+/-	EC
			dpm L^{-1}		µS cm^{-1}
0.5	153.7	6/2/11	22.6	9.5	36
0	153.7	6/2/11	3.2	2.8	36
0	152.7	6/1/11	24.1	7.0	36
0.5	156.6	6/5/11	5.4	3.7	14
0.5	156.6	6/5/11	4.1	4.8	15
0.5	156.7	6/5/11	17.1	3.0	12
0.5	156.7	6/5/11	17.2	5.3	12
0	157.7	6/6/11	4.3	3.0	44
0	157.7	6/6/11	6.5	5.3	45
0.5	158.3	6/7/11	4.8	3.1	21
0.5	159.2	6/8/11	3.8	2.1	37
0.5	159.3	6/8/11	9.7	5.4	36
0.5	153.7	6/2/11	8.2	5.7	42
0.5	153.7	6/2/11	20.5	5.5	50
0.5	162.7	6/11/11	1.6	1.1	16
0.5	162.7	6/11/11	3.3	1.2	16
0.5	165.0	6/14/11	4.9	6.9	35
0.5	165.5	6/14/11	5.4	2.1	27
0	166.7	6/15/11	3.2	2.1	23
0	166.7	6/15/11	10.7	5.8	23
0.5	167.5	6/16/11	2.7	1.1	18
1	167.6	6/16/11	2.7	3.2	18
1	170.0	6/19/11	3.8	1.1	12
1	170.0	6/19/11	4.3	1.8	12
0	172.7	6/21/11	2.7	2.7	14
0	172.7	6/21/11	4.8	4.7	14
0	184.6	7/3/11	2.1	0.9	
1	198.9	7/17/11	1.6	2.0	

660

661

662 **References**

663 Andrews, L.C., Catania, G.A., Hoffman, M.J., Gulley, J.D., Luthi, M.P., Ryser, C.,
664 Hawley, R.L., Neumann, T.A., 2014. Direct observations of evolving subglacial
665 drainage beneath the Greenland Ice Sheet. Nature 514, 80–83.

666 Bartholomew, I., Nienow, P., Sole, A., Mair, D., Cowton, T., King, M.A., 2012. Short-
667 term variability in Greenland Ice Sheet motion forced by time-varying meltwater
668 drainage: Implications for the relationship between subglacial drainage system
669 behavior and ice velocity. J. Geophys. Res. Earth Surf. 117.
670 doi:10.1029/2011JF002220

671 Bartholomew, I., Nienow, P., Sole, A., Mair, D., Cowton, T., Palmer, S., Wadham, J.,
672 2011a. Supraglacial forcing of subglacial drainage in the ablation zone of the
673 Greenland ice sheet. Geophys. Res. Lett. 38. doi:10.1029/2011GL047063

674 Bartholomew, I.D., Nienow, P., Sole, A., Mair, D., Cowton, T., King, M.A., Palmer, S.,
675 2011b. Seasonal variations in Greenland Ice Sheet motion: Inland extent and
676 behavior at higher elevations. Earth Planet. Sci. Lett. 307, 271–278.

677 Bhatia, M.P., Das, S.B., Kujawinski, E.B., Henderson, P., Burke, A., Charette, M.A.,
678 2011. Seasonal evolution of water contributions to discharge from a Greenland
679 outlet glacier: insight from a new isotope-mixing model. J. Glaciol. 57, 929–941.

680 Borges, A.V., Vanderborght, J.-P., Schiettecatte, L.-S., Gazeau, F., Ferrón-Smith, S.,
681 Delille, B., Frankignoulle, M., 2004. Variability of the gas transfer velocity of CO_2
682 in a macrotidal estuary (the Scheldt). Estuaries 27, 593–603.

683 Boulton, G.S., Hagdorn, M., Maillot, P.B., Zatsepin, S., 2009. Drainage beneath ice
684 sheets: groundwater–channel coupling, and the origin of esker systems from former
685 ice sheets. Quat. Sci. Rev. 28, 621–638.

686 Burnett, W.C., Dulaiova, H., 2003. Estimating the dynamics of groundwater input into
687 the coastal zone via continuous radon-222 measurements. J. Environ. Radioact. 69,
688 21–35.

689 Chandler, D.M., Wadham, J.L., Lis, G.P., Cowton, T., Sole, A., Bartholomew, I., Telling,
690 J., Nienow, P., Bagshaw, E.B., Mair, D., 2013. Evolution of the subglacial drainage
691 system beneath the Greenland Ice Sheet revealed by tracers. Nat. Geosci. 6, 195–
692 198.

693 Chandler, D.M., Wadham, J.L., Nienow, P.W., Hawkings, J., Doyle, S.H., Telling, J.,
694 Tedstone, A., Hubbard, A., Rapid growth and persistence of efficient subglacial
695 drainage under kilometre thick Greenland ice. Submitted.

696 Chanyotha, S., Kranrod, C., Burnett, W.C., 2014. Assessing diffusive fluxes and pore
697 water radon activities via a single automated experiment. J. Radioanal. Nucl. Chem.
698 1–8.

699 Charette, M.A., Buesseler, K.O., Andrews, J.E., 2001. Utility of radium isotopes for
700 evaluating the input and transport of groundwater-derived nitrogen to a Cape Cod
701 estuary. Limnol. Oceanogr. 46, 465–470.

702 Charette, M.A., Moore, W.S., Burnett, W.C., 2008. Uranium-and thorium-series nuclides
703 as tracers of submarine groundwater discharge. U-Th Ser. nuclides Aquat. Syst.
704 Elsevier 155–191.

705 Collins, D.N., 1979. Hydrochemistry of meltwaters draining from an alpine glacier. Arct.
706 Alp. Res. 307–324.

707 Cook, P.G., Favreau, G., Dighton, J.C., Tickell, S., 2003. Determining natural
708 groundwater influx to a tropical river using radon, chlorofluorocarbons and ionic
709 environmental tracers. J. Hydrol. 277, 74–88.

710 Corbett, D.R., Burnett, W.C., Cable, P.H., Clark, S.B., 1998. A multiple approach to the
711 determination of radon fluxes from sediments. J. Radioanal. Nucl. Chem. 236, 247–
712 253.

713 Cowton, T., Nienow, P., Bartholomew, I., Sole, A., Mair, D., 2012. Rapid erosion
714 beneath the Greenland ice sheet. Geology 40, 343–346.

715 Cowton, T., Nienow, P., Sole, A., Wadham, J., Lis, G., Bartholomew, I., Mair, D.,
716 Chandler, D., 2013. Evolution of drainage system morphology at a land-terminating
717 Greenlandic outlet glacier. J. Geophys. Res. Earth Surf. 118, 29–41.

718 Creyts, T.T., Schoof, C.G., 2009. Drainage through subglacial water sheets. J. Geophys.
719 Res. Earth Surf. 114.

720 Das, S.B., Joughin, I., Behn, M.D., Howat, I.M., King, M. a, Lizarralde, D., Bhatia, M.P.,
721 2008. Fracture propagation to the base of the Greenland Ice Sheet during
722 supraglacial lake drainage. Science 320, 778–81. doi:10.1126/science.1153360

723 Dow, C.F., Hubbard, A., Booth, A.D., Doyle, S.H., Gusmeroli, A., Kulessa, B., 2013.
724 Seismic evidence of mechanically weak sediments underlying Russell Glacier, West
725 Greenland. Ann. Glaciol. 54, 135–141. doi:10.3189/2013AoG64A032

726 Dulaiova, H., Burnett, W.C., 2006. Radon loss across the water-air interface (Gulf of
727 Thailand) estimated experimentally from ^{222}Rn-^{224}Ra. Geophys. Res. Lett. 33.
728 doi:10.1029/2005GL025023

729 Dulaiova, H., Gonneea, M.E., Henderson, P.B., Charette, M.A., 2008. Geochemical and
730 physical sources of radon variation in a subterranean estuary—implications for
731 groundwater radon activities in submarine groundwater discharge studies. Mar.
732 Chem. 110, 120–127.

733 Gonneea, M.E., Morris, P.J., Dulaiova, H., Charette, M.A., 2008. New perspectives on
734 radium behavior within a subterranean estuary. Mar. Chem. 109, 250–267.

735 Gulley, J.D., Benn, D.I., Screaton, E., Martin, J., 2009. Mechanisms of englacial conduit
736 formation and their implications for subglacial recharge. Quat. Sci. Rev. 28, 1984–
737 1999.

738 Hawkings, J.R., Wadham, J.L., Tranter, M., Raiswell, R., Benning, L.G., Statham, P.J.,
739 Tedstone, A., Nienow, P., Lee, K., Telling, J., 2014. Ice sheets as a significant
740 source of highly reactive nanoparticulate iron to the oceans. Nat. Commun. 5.
741 doi:10.1038/ncomms4929

742 Henriksen, N., Higgins, A.K., Kalsbeek, F., Pulvertaft, T.C.R., 2009. Greenland from
743 Archaean to Quaternary: descriptive text to the 1995 geological map of Greenland,
744 1: 2 500 000. Geological Survey of Denmark and Greenland.

745 Hindshaw, R.S., Rickli, J., Leuthold, J., Wadham, J., Bourdon, B., 2014. Identifying
746 weathering sources and processes in an outlet glacier of the Greenland Ice Sheet
747 using Ca and Sr isotope ratios. Geochim. Cosmochim. Acta 145, 50–71.

748 Hofmann, H., Gilfedder, B.S., Cartwright, I., 2011. A novel method using a silicone
749 diffusion membrane for continuous ^{222}Rn measurements for the quantification of
750 groundwater discharge to streams and rivers. Environ. Sci. Technol. 45, 8915–8921.

751 Hubbard, B., Sharp, M., Nielsen, M., Willis, I.C., Smart, C.C., 1995. Borehole water-
752 level variations and the structure of the subglacial hydrological system of Haut
753 Glacier d' Rolla, Valais, Switzerland. J. Glaciol. 41, 572–583.

754 Kies, A., Nawrot, A., Tosheva, Z., Jania, J., 2011. Natural radioactive isotopes in glacier
755 meltwater studies. Geochem. J. 45, 423–429.

Kies, a., Hengesch, O., Tosheva, Z., Nawrot, a. P., Jania, J., 2015. Overview on radon measurements in Arctic glacier waters. Cryosph. Discuss. 9, 2013–2052. doi:10.5194/tcd-9-2013-2015

McCallum, J.L., Cook, P.G., Berhane, D., Rumpf, C., McMahon, G.A., 2012. Quantifying groundwater flows to streams using differential flow gaugings and water chemistry. J. Hydrol. 416, 118–132.

Meierbachtol, T., Harper, J., Humphrey, N., 2013. Basal drainage system response to increasing surface melt on the Greenland Ice Sheet. Science 341, 777–779.

Nghiem, S. V, Hall, D.K., Mote, T.L., Tedesco, M., Albert, M.R., Keegan, K., Shuman, C.A., DiGirolamo, N.E., Neumann, G., 2012. The extreme melt across the Greenland ice sheet in 2012. Geophys. Res. Lett. 39.

Niu, Y., Clara Castro, M., Aciego, S.M., Hall, C.M., Stevenson, E.I., Arendt, C.A., Das, S.B., 2015. Noble gas signatures in Greenland: Tracing glacial meltwater sources. Geophys. Res. Lett. 42, 9311–9318. doi:10.1002/2015GL065778

Nye, J.F., 1973. Water at the bed of a glacier, in: International Association of Scientific Hydrologists Publication, 95. pp. 189–194.

Raiswell, R., 1984. Chemical models of solute acquisition in glacial meltwaters. J. Glaciol. 30, 49–57.

Rempel, A.W., 2009. Transient effective stress variations forced by changes in conduit pressure beneath glaciers and ice sheets. Ann. Glaciol. 50, 61–66.

776 Röthlisberger, H., 1972. Water Pressure in Intra-and Subglacial Channels: Pres. at the
777 Symposium on the Hydrology of Glaciers, 7-13 September 1969, Cambridge.

778 Schoof, C., 2010. Ice-sheet acceleration driven by melt supply variability. Nature 468,
779 803–806.

780 Schubert, M., Paschke, A., Bednorz, D., Bürkin, W., Stieglitz, T., 2012. Kinetics of the
781 water/air phase transition of radon and its implication on detection of radon-in-water
782 concentrations: practical assessment of different on-site radon extraction methods.
783 Environ. Sci. Technol. 46, 8945–8951.

784 Sharp, M., Richards, K., Willis, I., Arnold, N., Nienow, P., Lawson, W., Tison, J., 1993.
785 Geometry, bed topography and drainage system structure of the Haut Glacier
786 d'Arolla, Switzerland. Earth Surf. Process. Landforms 18, 557–571.

787 Sole, A., Nienow, P., Bartholomew, I., Mair, D., Cowton, T., Tedstone, A., King, M.A.,
788 2013. Winter motion mediates dynamic response of the Greenland ice sheet to
789 warmer summers. Geophys. Res. Lett. 40, 3940–3944.

790 Tedstone, A.J., Nienow, P.W., Sole, A.J., Mair, D.W.F., Cowton, T.R., Bartholomew,
791 I.D., King, M.A., 2013. Greenland ice sheet motion insensitive to exceptional
792 meltwater forcing. Proc. Natl. Acad. Sci. 110, 19719–19724.

793 Tranter, M., 1993. A conceptual model of solute acquisition by Alpine glacial
794 meltwaters. J. Glaciol. 39.

795 Tranter, M., Sharp, M.J., Brown, G.H., Willis, I.C., Hubbard, B.P., Nielsen, M.K., Smart,
796 C.C., Gordon, S., Tulley, M., Lamb, H.R., 1997. Variability in the chemical
797 composition of in situ subglacial meltwaters. Hydrol. Process. 11, 59–77.
798 doi:10.1002/(SICI)1099-1085(199701)11:1<59::AID-HYP403>3.0.CO;2-S

799 Walder, J.S., 1986. Hydraulics of subglacial cavities. J. Glaciol 32, 439–445.

800 Werder, M.A., Hewitt, I.J., Schoof, C.G., Flowers, G.E., 2013. Modeling channelized and
801 distributed subglacial drainage in two dimensions. J. Geophys. Res. Earth Surf. 118,
802 2140–2158.